The Deep Autonomous Profiler (DAP), a Platform for Hadal Profiling and Water Sample Collection

LILLIAN MUIR,[a] CHRIS ROMAN,[a] DAVID CASAGRANDE,[a] AND STEVEN D'HONDT[a]

[a] *University of Rhode Island, Narragansett, Rhode Island*

(Manuscript received 17 August 2020, in final form 2 July 2021)

ABSTRACT: The Deep Autonomous Profiler (DAP) is a full-ocean-depth profiler rated to 11 km. Its hydrographic profiles and water samples can provide information on physical oceanographic properties, seawater composition, and biological communities at every depth in the ocean. Designed around a 24-bottle rosette, the DAP is an untethered system able to autonomously collect temperature, salinity, and oxygen profiles, as well as water samples. An adaptive sampling method was developed to analyze the water-column data to identify and sample desired features while under way. Acoustic ranging-only tracking is used to monitor and geolocate the system underwater. In September 2018 the vehicle was tested to 8377 m in the Puerto Rico Trench. The DAP was able to generate full-ocean-depth profiles and collect water samples at both preset and adaptively determined depths. To demonstrate the utility of the DAP, we radiocarbon dated the deepest water sampled in the Puerto Rico Trench, providing the first direct evidence of hadal water-mass age in the trench: 318 ± 25 yr. This paper presents an overview of the DAP system and the Puerto Rico Trench sea trials.

KEYWORDS: Ocean; North Atlantic Ocean; Instrumentation/sensors; Profilers, oceanic; Sampling; Automated systems

1. Introduction

Studies of hadal seawater and its biological communities are historically difficult to obtain and rare. Measuring and sampling the hadal ocean will provide insight into a host of physical and biological processes. The processes that dominate ocean mixing in deep trenches are not fully known, because measurements of physical processes and water-mass ages are rare (Taira et al. 2004; Schmidt and Siegel 2011). The nature of planktonic communities in deep trenches is also largely unknown. Deep-sea trenches have been described as inverted islands of biodiversity, because hadal animal species are often restricted to a single trench or adjacent trenches by the fact that the ocean is mostly continuous at abyssal depths but not generally continuous at hadal depths from trench to trench (Vinogradova 1997). Recent studies of prokaryotic plankton in the Mariana Trench show that hadal water contains distinct communities relative to the overlying abyssal water (Nunoura et al. 2015; Tarn et al. 2016; Peoples et al. 2018). However, the full nature of planktonic biodiversity in trenches, including the extent to which hadal plankton are restricted to individual trenches, remains unclear because studies of hadal plankton are so rare.

These broad unknowns within hadal studies are related to the numerous challenges that make directly measuring phenomena, such as deep-water mixing, and sampling biological communities at hadal water depths difficult. The most common ship profiling and sampling device is a conductivity–temperature–depth (CTD) rosette system made up of a sensor system (e.g., Sea-Bird SBE 9plus) and a rosette of sampling bottles (e.g., Sea-Bird SBE 32) (Millard and Yang 1993). Rosettes are typically tethered systems lowered over the side of a ship with a wire and winch for real-time communication and data acquisition (Franks and Keafer 2003).

While operating, the CTD wire needs to handle the static and dynamic loads on the system. The weight of the cable must be considered as a part of the static load, and it increases as more wire is spooled out. A common wire for CTD systems is 0.322-in.-diameter (1 in. = 2.54 cm) electromechanical cable, which weighs 0.215 kg m^{-1} in seawater and adds an extra 1290 kg for a 6000-m cast. This extra weight will increase the load close to the safe working limits for the system [University-National Oceanographic Laboratory Systems (UNOLS); UNOLS 2015]. Larger-diameter steel wires or specialized synthetic materials can be used but have similar problems because they either weigh more per unit length or are costly. As a result of these wire limitations, shipboard rosettes are not typically used below 6000 m and are unable to sample the hadal zone.

Shipboard CTDs can operate at vertical speeds up to 60 m min^{-1}. A full 6000-m profile takes 2 h or more to descend and takes longer to ascend because of sampling stops (Crease et al. 1988). A shipboard CTD also requires the vessel to maintain station over a site and several dedicated personnel to be involved in the operation. Given the operating costs of scientific vessels, a deep CTD cast is an expensive activity.

To circumvent the wire limitations, free-falling landers are the main platforms for sampling the hadal ocean. Landers are untethered, adaptable platforms that sink and land on the ocean floor (Cui et al. 2014; Hardy et al. 2013). Expendable weights are typically mounted to the bottom of the vehicles for the descent, while syntactic foam or glass spheres are used for buoyancy to return the system after the weights are released (Jamieson et al. 2009). As research platforms, landers can easily be equipped for a variety of tasks at a low cost. Lander instrumentation commonly includes camera systems, water samplers, sediment cores, CTD sensors, and baited traps. Because of this versatility, most deep-sea exploratory programs like Deepsea

Corresponding author: Chris Roman, croman2@uri.edu

DOI: 10.1175/JTECH-D-20-0139.1

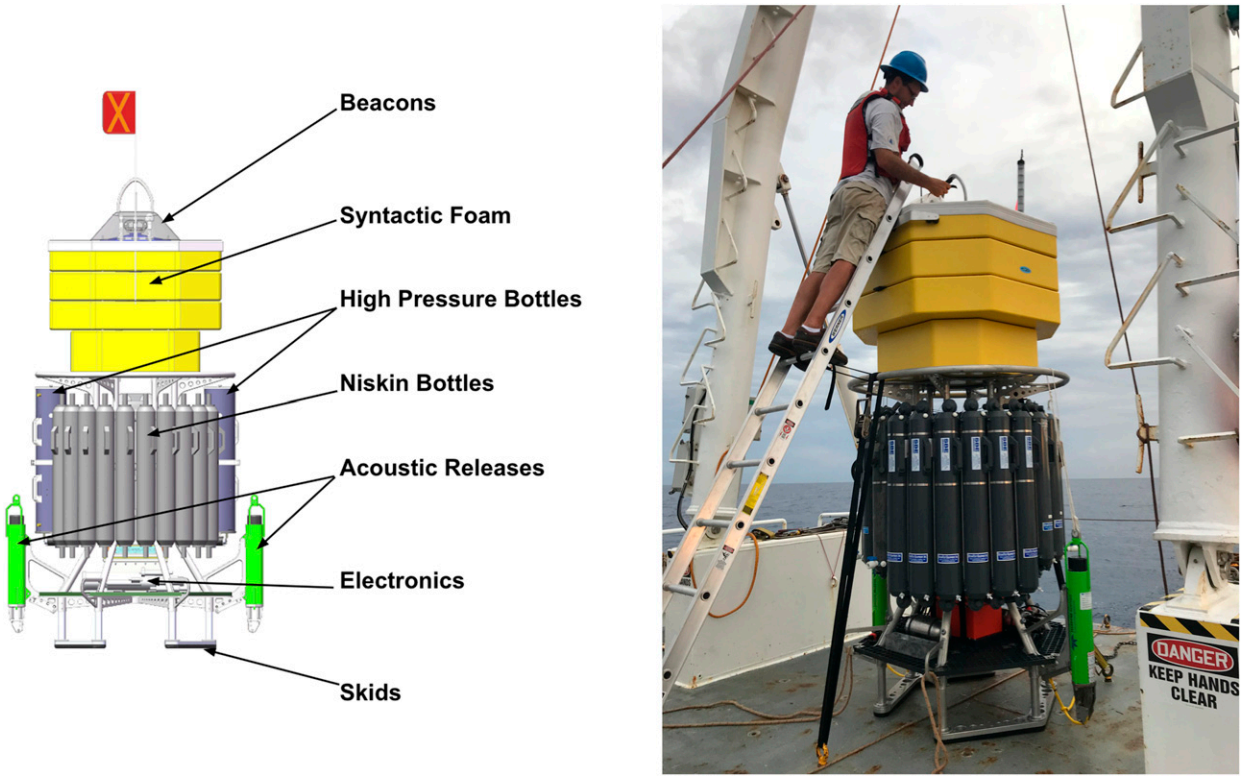

FIG. 1. The DAP vehicle: (a) a labeled diagram of the DAP CAD model and (b) a photograph of the vehicle being prepared for a dive.

Challenge, Hadal Environment and Educational Program (HADEEP), and Hadal Ecosystems Studies (HADES) use landers as the primary data collection sources (Jamieson et al. 2009; Hardy et al. 2013; Linley et al. 2016).

Few remote or human-occupied research vehicles have ventured to the hadal region. The successful vehicles include the Deepsea Challenger (Gallo et al. 2015), Nereus (Bowen et al. 2008), Kaiko (Kyo et al. 1995), and Automatic Bottom Inspection and Sampling Mobile (ABISMO) (Ishibashi et al. 2008). The primary purpose of deep vehicles is bottom exploration. They are more capable than landers and attempt to document the environment through video, still imagery, biologic samples, geologic samples, bathymetric mapping, CTD data, and small water samples (Bowen et al. 2009; Yoshida 2009). Two of these systems managed to make only a few dives to the hadal region before being lost (Kaiko and Nereus) and others have been retired (Deepsea Challenger and ABISMO) (Momma et al. 2004; Showstack 2014).

The Deep Autonomous Profiler (DAP) presented here is a combination of a CTD rosette and a free-falling lander. It is able to profile the water column, collect large quantities of nonpressurized water (twenty-four 12-L bottles), and collect small pressure-retaining samples (135 mL each). The system is controlled by an onboard data collection and sampling algorithm that enables preset and adaptive sample collection, based on target values of measured or derived parameters.

Adaptive sampling methods, which allow a sampler or vehicle to make data-driven decisions, are being increasingly utilized in oceanography, because of the spatiotemporal variability of the environment (Das et al. 2015; Fossum et al. 2019). Yilmaz et al. (2008) and Lermusiaux (2007) discuss the necessity, theory, and methods behind adaptive sampling based on current data (nowcast), predicted data (forecast), or past data (hindcast) to inform a sampling strategy. Most adaptive sampling studies attempt to locate, sense, and sample interesting environmental features. Studies using gliders or multiple autonomous underwater vehicles achieve this objective by using adaptive software to navigate and plan paths (Yilmaz et al. 2008; Lermusiaux 2007; Popa et al. 2004; Leonard et al. 2010).

DAP concept

The DAP was designed to expand the capabilities of a CTD system to the full ocean depth (11 km) by removing the constraints associated with wire-based operations. Removing the tether allows the vehicle to autonomously profile and sample seawater into the hadal region. Because it only requires the ship for deployment and retrieval, use of the DAP allows the ship to perform other tasks while the DAP is under way. The only source of communication to the DAP while deployed are the acoustic releases. These provide a range value that can be used with a motion model to estimate the location of the DAP.

The DAP is built around a 24-bottle Sea-Bird SBE 32 rosette for 10- or 12-L Niskin bottles (Fig. 1). The large aluminum bottle-support rings from the standard rosette were modified to reduce weight and are held by the vehicle's custom frame. Similar to many lander designs, the DAP uses syntactic foam to

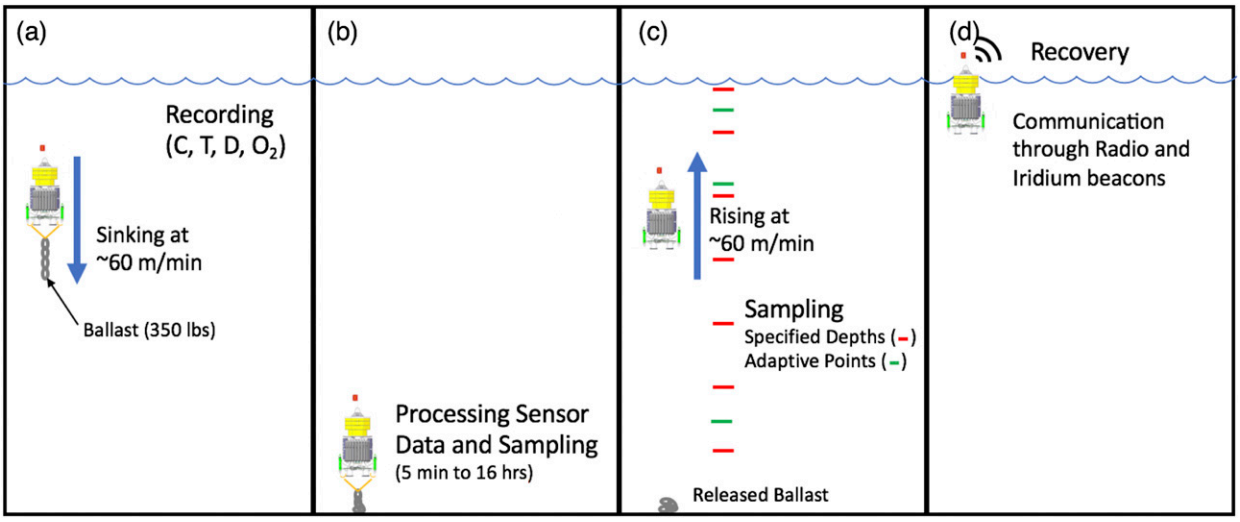

FIG. 2. Depiction of DAP autonomous operation and sampling showing it (a) during the descent, (b) parked on the sea floor, (c) during the ascent, and (d) surfaced.

provide buoyancy for the ascent and drop weights for descent. The syntactic foam has a density of 670 kg m^{-3} and was selected instead of glass sphere flotation for several reasons. The foam flotation is more space efficient than multiple glass balls, and foam does not require routine inspections for internal spalling that can occur in glass with repeat cycling to high pressure. In addition, the DAP was designed to be deployed and recovered as a single unit, which is not possible with designs that use a vertical string of spheres connected with line or chain.

Because of this design, DAP is set up to efficiently conduct multiple full-ocean-depth dives with easy deployment and recovery. Unlike most other deep-sea vehicles, the DAP focuses on water-column profiling and sampling. This system provides a water-column profile and is the first to be able to efficiently retrieve large volume hadal water samples. It is rated for a full ocean depth of 11 km and can be reconfigured with different sensors or sampling devices. This adaptability and efficiency allow for a broad range of oceanographic studies in deep-water environments. For example, it can be used to determine deep-water mixing and water overturn rate in ocean trenches through radiocarbon dating around the globe with large water samples from successive and repeatable dives. To demonstrate this capability, an analysis on the deep-water mixing and the radiocarbon age of the Puerto Rico Trench Bottom Water was performed.

The remainder of this paper provides more details on the DAP system and initial testing results. Section 2 presents a system description and operation details. Section 3 describes the initial hadal testing and provides results from deployments in the Puerto Rico Trench during September 2018. Section 4 summarizes the paper and provides insight toward the next steps of this project.

2. DAP system design

The vehicle's frame is made of aluminum to reduce weight, while being strong enough to support the syntactic foam and 24 full Niskin bottles during recovery. Fiberglass grating on the lower platform, plastic bottle supports, and bottom skids were selected to reduce the in-water weight. In total, 1.03 m^3 of foam is used to provide sufficient buoyancy with some margin for adding additional sensors in the future. The DAP stands 3.2 m tall and has a mass of approximately 1400 kg in air empty and 1700 kg when full of water. The titanium electronics bottle, tested to 11 960 dBar in a pressure facility, was designed to house the embedded Raspberry Pi computer and power circuitry. This computer logs data from the SBE 9plus CTD and SBE 43 oxygen sensor, sends commands to the SBE 32 sampler carousel to trigger the sample bottles, and controls the burn-wire release. Power for a nominal 24-h operating time is provided by a 24-V, 40-A h oil-filled DeepSea Power and Light SeaBattery. Longer-duration dives with burst sampling and computer power-downs would be possible but have not been implemented yet. Two Benthos acoustic releases, mounted low on the outside of the vehicle, are used for redundancy. This location keeps the center of gravity low, makes rigging the releases easy, ensures one beacon has line of site to the ship for communications and tracking, and keeps the beacons deep enough to maintain useful communication when the vehicle is floating at the surface.

Figure 2 shows the operational steps of the DAP. Using drop weights, the profiler descends at a nominal speed of 60 m min^{-1} through the water column, collecting CTD data. Upon reaching the bottom, a timer is activated and an onboard algorithm processes the descent profile to set the trigger depths for any sample bottles set with an adaptive criteria. Bottom water samples can also be collected according to any preset delays. The bottom time can vary anywhere from 5 min (quick profile) to 18 h (time-lapse bottom sampling), depending on the objective of each dive and the amount of time allocated to the ascent and descent. A burn wire is used to release the drop weights when the planned bottom time limit is reached. During the ascent, at a nominal speed of 60 m min^{-1}, the Niskin bottles are triggered at any preset depths specified in the mission file or

at adaptively calculated depths based on downcast data. When the DAP surfaces, a radio beacon, Iridium beacon, strobe, radar reflector, and flag are used for recovery by the ship.

The vehicle can currently hold up to 24 Niskin bottles, and up to four pressure-maintaining sample bottles provided by the Scripps Institution of Oceanography (Peoples et al. 2019). The Niskin bottles can sample large quantities of water throughout the water column but depressurize on the ascent. The Scripps samplers take small (135 mL) samples and hold them at high pressure. Each high-pressure sampler is enclosed in a schedule 80 PVC pipe (internal diameter of 19.3 cm) thermal water jacket to keep the sampler cold during the ascent and recovery. The jackets have an internal length of 96.5 cm and hold approximately 25 L of water. The inside of the tubes are lined with thick faux sheepskin carpet to reduce internal water motion and convection. During our test deployments, these jackets were able to keep the sampler temperature below 8°C at recovery, despite the DAP drifting in surface water of 29°C for up to 45 min during recoveries. On short deployments, where the water in the jacket may not have enough time to acclimate to bottom temperature, the jackets can be filled with cold water prior to deployment. Because of the size of the thermal jackets, each high pressure sampler takes the place of two Niskin bottles.

Expendable steel drop weights, typically 140–180 kg per dive, are attached for the descent of each dive and are released on the bottom to allow the system to float back to the surface. This much weight produces vertical speeds around 60 m min^{-1}, depending on the exact configuration of the sample bottles. For redundancy, four independent release mechanisms are able to drop the weight, which hangs below the vehicle's base on a length of 0.25-in. chain. Hanging the weights ~3 m below the vehicle provides enough distance for the roughly 1 m of overshoot that is due to the vehicle's momentum after the weights hit the bottom. This distance also provides some forgiveness if the bottom is very soft and significantly reduces the chance of the vehicle becoming stuck in the sediment.

Launching the vehicle is a four-step process that takes just a few minutes. First, the descent weights are put over the side of the ship and held with a temporary slip line attached near the top of the expendable chain. Second, the DAP is positioned at the edge of the deck with a standard pull-pin release connected to the vehicle's titanium lifting bale. Third, the top end of the weight chain is attached to the DAP's release rigging and the slip line is released to transfer the load to the DAP. Fourth, the DAP is put over the side and released with the pull pin.

The primary release mechanism for recovery is a burn wire activated by a software timer. Energizing the burn-wire circuit causes the wire to dissolve in seawater and release the weights. The two Benthos acoustic releases can be activated through an acoustic command sent from a shipboard transducer and will send a confirmation status signal to indicate they have released. The fourth fail-safe release mechanism is a passive corroding galvanic link. This link slowly dissolves when exposed to saltwater and can be sized for different dive durations. In the event of a burn-wire software failure and a loss of acoustic communication, the galvanic link will eventually corrode to release the weights.

Upon surfacing, several beacons are used to locate the DAP for recovery. A radio frequency beacon and an Iridium beacon activate upon surfacing. The radio direction finder can be used to determine the bearing to the vehicle relative to the ship. The Iridium beacon obtains the GPS coordinates of the system and sends the position via email over satellite. To increase visibility, an orange flag and a radar reflector stick a few feet above the surface. A strobe is used for night recoveries. A clear acrylic cover keeps the beacons from being snagged on the launch or recovery line.

a. Sampling methods

The trigger conditions to close each bottle are set in a mission plan before each dive. The operator can use a combination of depth sampling, bottom time delay sampling, and adaptive sampling based on the recorded CTD and oxygen data. The vehicle software identifies the bottles by the "bottle ID" number, a "trigger" parameter, a "value" to close the bottle, and the "state" in which the vehicle should be when the bottle closes. The state options ("down," "bottom," "up," "surface") are determined by monitoring changes in velocity and depth over time.

1) DEPTH SAMPLING

Depth sampling is the primary method for triggering bottles. This method can provide samples throughout the profile to get a representation of the water column similar to a shipboard CTD cast (Fig. 3). In this mode, the operator sets the trigger for a bottle as "depth." The value is entered as the specific depth the bottle should close, bottom or surface. The default state is up, to close the bottle during the ascent, but can be set to down if desired. Bottles can be triggered in the bottom state with a time delay. The "delay" value is relative to when the vehicle first lands on the bottom and allows for a time series of bottom water samples.

2) ADAPTIVE SAMPLING

The adaptive sampling mode is designed to compliment the depth-specific samples by locating and sampling at distinct features in the water column. Preset depth sampling has a high likelihood of missing key water features like minimums, maximums, or gradients. The adaptive algorithm analyzes the downcast data while on the bottom (Fig. 2b) to generate target depths for the ascent. The user can set parameters for trigger, value, range window, and offset. These describe which data source to use, the portion of the water column to consider, and the value at which to collect a sample. The state will always be up for the adaptive bottles because the descent profile is needed to find the water-column features.

The trigger parameter is the water property to be examined for the water-column feature. This parameter is limited to the sensors on the DAP during sampling. For the Puerto Rico tests, the triggers were salinity, temperature, oxygen, and density.

The trigger parameter can be narrowed using the range window. This is an optional parameter that allows the profile to be parsed into depth ranges set by upper and lower depth bounds. The possible inputs include "surface," "middle," "bottom," or a user-specified depth range. The range window

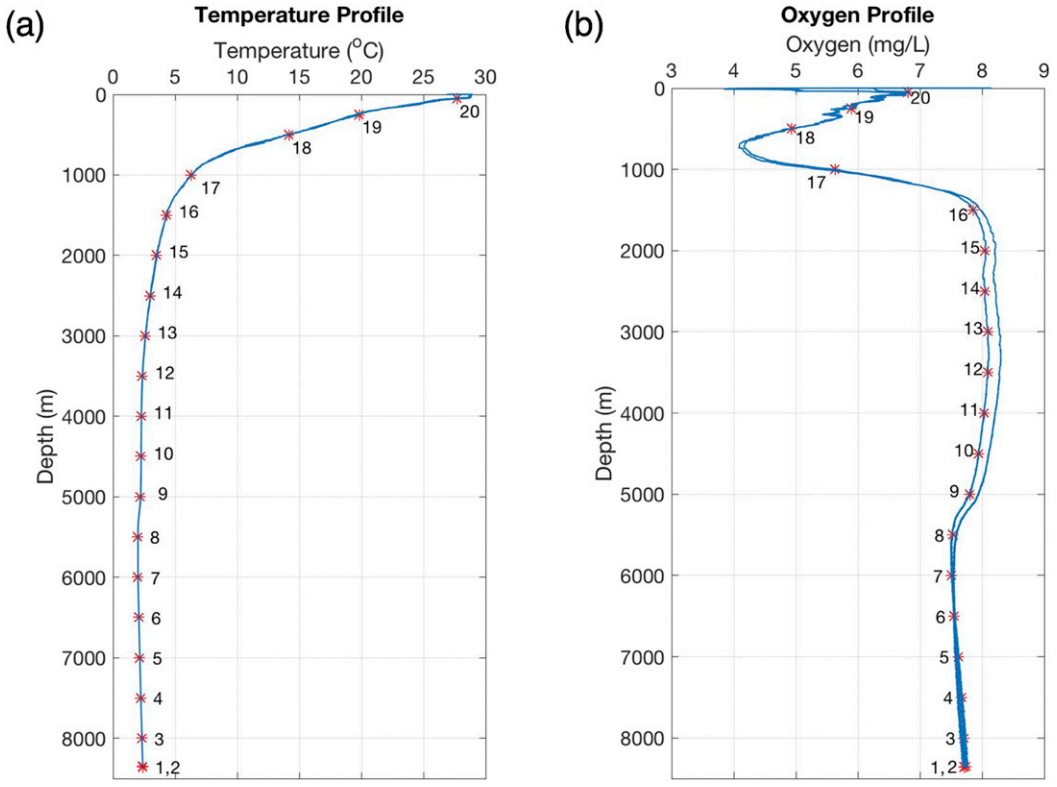

FIG. 3. Depth sampling distribution of 20 bottles spread through the water column at 500-m intervals to provide a representative sampling of the entire water column. The bottle depths are displayed on (a) temperature and (b) oxygen profiles from the Puerto Rico Trench.

allows smaller changes in the profile to be identified, especially smaller gradients and local maxima or minima. The default for the range window is the entire profile, surface to bottom, where the surface parameter is actually set to 50 m, or another shallow depth, to avoid the complexity of the surface layer. In practice, knowledge of the water column from previous dives or CTD casts allows the range window to be set with increasing specificity to enable sampling more subtle features in the water column.

The value parameter indicates how the trigger parameter will be analyzed within the range window. Value can be set to "minimum," "maximum," "gradient," or a specific value to find in the profile. The gradient is calculated by first smoothing the data for the selected trigger parameter with a moving-average filter and then taking the derivative of the trigger parameter with respect to depth. The data array is smoothed with a square convolution function. A window length of 240 (24 samples per second for 10 s) is used to maintain the general trend of the curve but ignore any noise in the measurements that could cause a false trigger. Since all of the data are collected on the downcast, the smoothing is done with a symmetric window function to avoid a depth shift in the filtered signal.

Setting the value to gradient will take a sample at the largest change in the parameter, which may not be at the desired location because of the structure of the water column. The range window helps to avoid this by narrowing down the region of the water column to consider, such as looking below 500-m depth for the strongest gradient in the lower oxycline.

The offset parameter is a modification that can be used to move the sample depth shallower or deeper by a fixed amount relative to the calculated gradient depth. This allows for sampling water across the gradient and adds a measure of redundancy should the water column change between the decent and ascent phases of the dive.

This set of parameters generates a flexible profiling system that can be used to sample oxygen minimums, thermoclines, haloclines, local values, and adjacent water masses.

b. Operations

The Raspberry Pi running the DAP monitors the sensors, determines the state of the vehicle, calculates the adaptive sampling locations, activates the burn wire, and triggers the bottles to close when specified. The Linux-based software is written in Python and C and uses the Lightweight Communications and Marshalling (LCM) (Huang et al. 2010) library for interprocess communications and data logging. LCM operates using a publish/subscribe system with predefined data types and allows the major software components for sensor communications, mission execution, adaptive processing and sample acquisition to be separate and modular. For instance, the adaptive processing code could be modified or

entirely changed to handle additional sensors or methods independent of the other processes. LCM is also used on the ship to log the acoustic ranges to the Benthos releases and any ship positioning data.

1) MISSION PLANNING

Before each deployment, the user writes a mission plan to dictate the sampling instructions and timing. The mission plan is made up of global parameters for the dive and the previously described sample bottle descriptors. An example mission plan is provided in the appendix. The dive is described by the global parameters of bottom time and system launch latitude. The other global parameters set abort conditions that cause the burn wire to activate and release the weights. These include the maximum mission time, the maximum depth, a battery cutoff, and a CTD communications abort that will release the weights if a sensor fault occurs.

2) ACOUSTIC TRACKING

The two Teledyne Benthos R-Series releases are used for acoustic ranging. Using commands from the topside deck unit, the operator can check the status of the releases, send the release command, adjust the acoustic settings, and obtain range measurements. During testing, the DAP was monitored with range-only tracking. Figure 4 shows a full dive of ranges plotted against time as the ship loitered within roughly 3 km of the deployment site. The pattern of ranges indicates gaps during which no ranges were received and an alternating pattern of which beacon had a clear acoustic path to the ship.

The beacon transducer is omnidirectional, so there is no way to determine the location or bearing to the beacon from a single range. A rough estimate of the location can be calculated using multiple ranges, the ship's location, and a model of DAP's vertical motion. Such range-only navigation methods are common for underwater vehicle tracking and vary depending on the measurements available and the quality of any models that predict the vehicle motion relative to prior estimated positions (Stutters et al. 2008; Kinsey et al. 2006; Vaganay et al. 2000; Mandić et al. 2016). The unknowns in the DAP's implementation are the depth of the vehicle after deployment or once it has left the bottom for the ascent and the horizontal range to the vehicle relative to the ship.

The depth of the DAP can be estimated with a motion model using an assumed buoyancy, drag coefficient, and water-column density. Inputs to the model include the launch time, bottom time, and the anticipated vertical speeds at the surface and bottom. A graphical user interface allows the user to set the deployment and off-bottom times and adjust the parameters to fine-tune the model. Because of the seawater density change with depth, compression of the foam, and differences in the up and down drag coefficients, the vehicle speed varies with depth and direction. By evaluating several deployments with different ballasting, the downward and upward drag coefficients were calculated as 0.73 and 1.02, respectively, each with approximately a 5% error. For this calculation, the frontal area of the vehicle was specified as 1.56 m^2, which is the area within the upper frame ring that is largely blocked by the foam pack. During descent, it seems that the hanging ballast weights break

FIG. 4. Received ranges from the DAP while under way throughout an entire dive. Typically, one beacon had a better acoustic path as the ship moved around the dive location. There were also gaps in which no responses were received.

the flow and effectively extend the length of the vehicle to reduce the drag, while the blunt face of the foam increases drag for the ascent. Additionally, the foam is less compressible than seawater, resulting in an approximately 225 N increase in buoyancy at roughly 8000-m depth.

To simplify the speed calculations in the model, the speed profile is assumed to be linear between the surface and bottom, with each value initially estimated using the drag coefficients, water density, and ballast condition for each deployment. When an acoustic slant range to the vehicle is received, the model calculates the expected depth of the vehicle at that time and then calculates the horizontal range from the ship assuming the slant range, estimated depth, and horizontal range from a right triangle. Since no bearing information is available, the horizontal range defines a circle of potential locations around the ship. Repeating this process using multiple ranges collected from different ship locations will cause the horizontal range circles to overlap at fewer and fewer possible locations until there is only one likely position estimate. In practice, the estimated depth based on the model is used during the ascent and descent phases of the dive to get a rough estimate of the horizontal motion due to currents. Once the vehicle is on the bottom, as confirmed by a distinct flattening in the acoustic range versus times plot (Fig. 4), an estimated depth value can be used to refine the position while the vehicle remains on the bottom.

3. Field-testing results

The DAP was tested in the Puerto Rico Trench for a total of nine dives during September of 2018. The tests verified the vehicle's operations, checked the sensor accuracy at depth, and demonstrated the utility of the adaptive water sampling method.

a. Sensor analysis

The SBE 9plus CTD has an stated initial accuracy of 0.001°C and 0.3 mS m^{-1} at any pressure with a stability of 2×10^{-4} °C $month^{-1}$ and 0.3 mS m^{-1} $month^{-1}$. The Digiquartz pressure

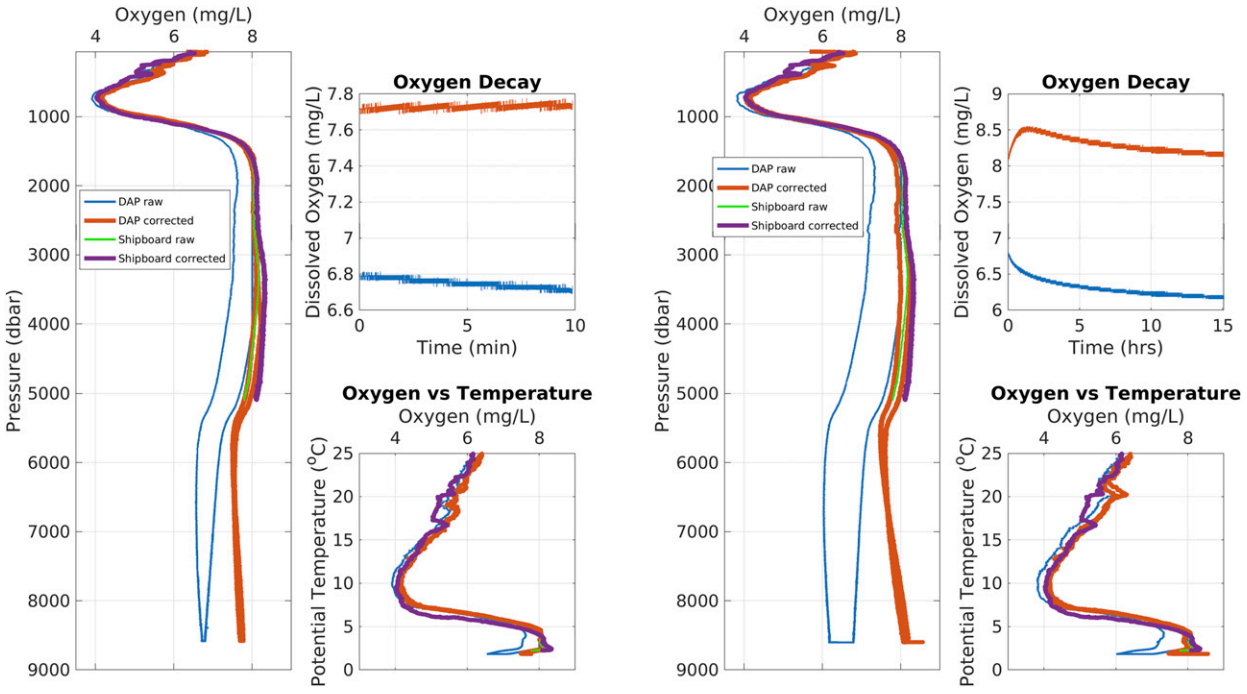

FIG. 5. Hysteresis correction comparison between the DAP raw and corrected oxygen data with the shipboard CTD raw and corrected oxygen data. (left) Correction plots for a short dive (10-min bottom time) with parameter values H1 = −0.037, H2 = 5000, and H3 = 2000. (right) Correction plots for a long dive (16-h bottom time) with parameter values H1 = −0.051, H2 = 5000, and H3 = 2200. For each side (group of three plots), the left plot shows oxygen profiles against depth, the top-right plot shows the initial and corrected readings while on the bottom, and the bottom-right plot shows the oxygen and temperature relationship.

sensor has an accuracy of 0.015% of full depth range. A comparison between the DAP and the shipboard CTD showed a mean difference of 0.021°C and 2.5 mS m^{-1} below the mixed layer down to 5000-m depth. This difference is reasonable given that the sensors were calibrated 6 months before the trip.

The SBE 43 oxygen sensor uses a permeable membrane to measure the dissolved oxygen in the water. Because of the plasticity of the membrane and a change in its permeability at pressure, the sensor experiences hysteresis, as shown in Fig. 5. Sea-Bird acknowledges this issue and has guidelines to correct for it (Edwards et al. 2010; Sea-Bird 2014) using tuning parameters (H1, H2, and H3) to bring the measurement closer to the actual value. When adjusting these constants, Sea-Bird suggests minimizing the hysteresis gap of oxygen against pressure and of oxygen against potential temperature while attempting to eliminate the decay of the oxygen measurement when the sensor is at a constant pressure, such as when sitting on the bottom.

The shipboard CTD's oxygen sensor (another SBE 43 oxygen sensor) was used as the tuning benchmark for the Puerto Rico tests. The thick red line on the plots (Fig. 5) shows the corrected profile using Sea-Bird's algorithm, and the thin green and thick purple lines show the shipboard CTD's raw and corrected data as a reference.

One issue with this correction method is that the pressure effect has a long time constant and the parameter values depend on the time–pressure history for each dive. For some dives during our tests the system remained on the bottom for hours, which affected the membrane more. As a result of this inconsistency, each dive needs the tuning variables to be adjusted based on the dive depth and time-at-pressure to remove the hysteresis. The hysteresis effect was much less noticeable for the shipboard CTD cast, which only went to 5000-m depth and immediately returned to the surface.

A potential remaining issue with the profile is the validity of the measured increase in oxygen below approximately 6000 m. Between 5000- and 6000-m depth, the reduction in temperature of 0.03°C and salinity change of 0.04 psu corresponds to the observed reduction in measured oxygen over that depth range. Beyond 6000 m the oxygen appears to increase linearly at different rates, depending on how much time the sensor was on the bottom (Fig. 5). This time dependence indicates that the increase is likely a sensor artifact that is not completely compensated for by the hysteresis correction. Unfortunately, the oxygen concentration was not directly measured in the collected high pressure samples for comparison. In addition, data from deep water in the Izu-Ogasawara Trench show a nearly constant oxygen concentration below 6000 m (Gamo and Shitashima 2018), which also suggests the increase we observed with depth in the Puerto Rico Trench is a sensor artifact.

b. Water sampling

During testing, the depth-triggered method was used to distribute the Niskin bottle samples evenly throughout the water column (Fig. 3). The software accurately triggered

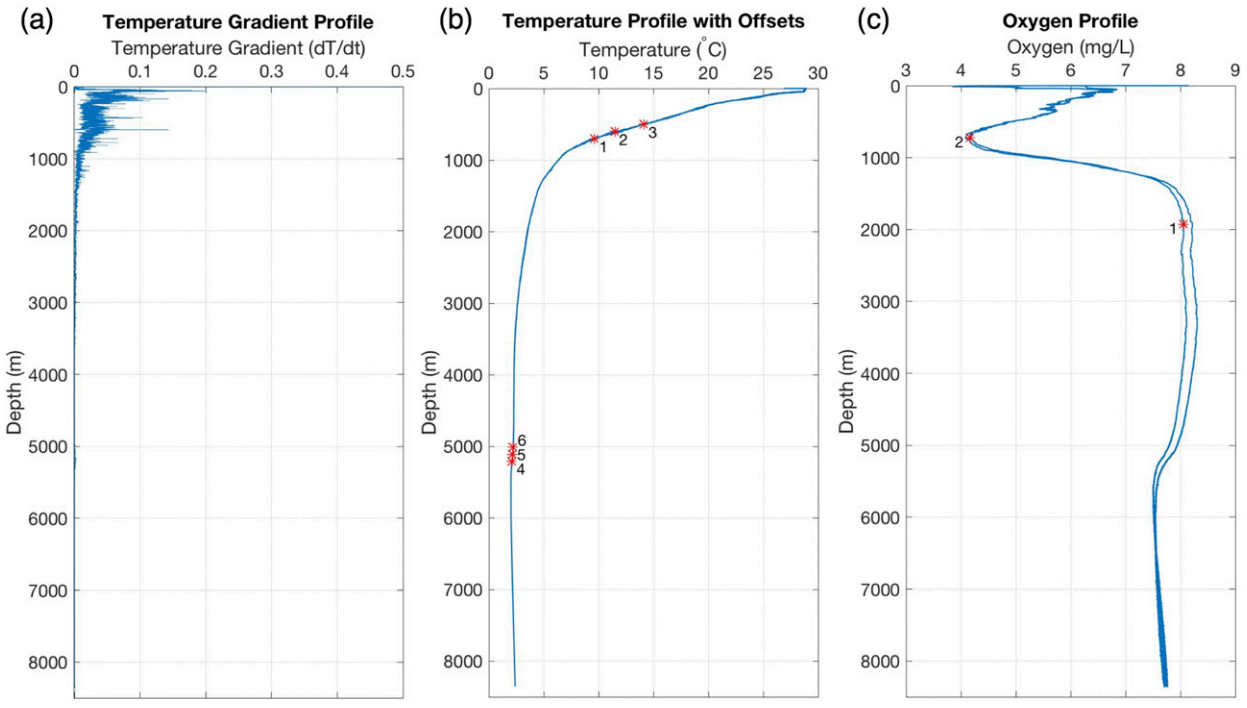

FIG. 6. Adaptive sampling examples: (a) temperature gradient profile used to identify gradient bottles to be sampled. (b) temperature sampling bottles at deep (bottle 5) and shallow (bottle 2) gradients with 100-m offsets around each gradient and (c) oxygen adaptive example of a maximum (bottle 1) and minimum (bottle 2).

bottles when the indicated depth was reached during the ascent. A slight sample lag of about 1 m is expected because of the continuous movement of the DAP and the typical delay in the SBE 32's action. The bottom time delay sampling was used during overnight deployments where the vehicle was parked for extended periods of time. The time series was collected to determine if sediment kicked up from the weights hitting the bottom was captured in the water samples. By taking samples upon impact and then with delays of 5, 10, 15, 30, 60 min, and each hour afterward, we observed the presence of sediment in the filtered water samples collected within the first hour after landing on the bottom.

The adaptive algorithm was first tested offline using data collected on previous deployments. This testing capability is embedded in the vehicle's operating software and any adaptive sampling scheme can be tested prior to deployment to confirm that the sample bottles will be triggered at the desired water-column features. The adaptive sampling method depends on minimal temporal change of the water column to sample features on the ascent after analyzing the downcast data. The comparison between the descent and ascent profiles below the mixed layer showed temperature and salinity differences less than 0.08°C and 0.01 psu. These small differences indicate the Puerto Rico Trench water column is sufficiently stationary over time for this sampling scheme.

The success of the adaptive sampling method used during a deployment can be seen in Fig. 6. The targeted temperature features were local maxima on the gradient plot in Fig. 6a. The main thermocline below the surface mixed layer was successfully sampled with bottle 2 in Fig. 6b. A hadal thermocline was identified by limiting the range window to 5000 m and below. Bottles 1, 3, 4, and 6 were taken with a 100-m offset to collect samples above and below the peak gradients. Figure 6c shows the sampling using the oxygen data. Bottles 1 and 2 were collected at the oxygen maximum and minimum, respectively.

Figure 7 shows the combination of the sampling methods. The red symbols indicate depth and bottom samples, and the black symbols show adaptive points of thermoclines (bottles 17 and 18), oxygen minimum (bottle 19), and salinity minimum (bottle 20). Each dive on the test cruise used a different combination of depth, time-based, and adaptive sampling to collect water from all areas of the profile. Overall, the adaptive system located and sampled the water-column features as desired. In practice, a user can use the offset and range window to refine the sampling and compensate for any variability in the water column.

c. *Deep-water sample analysis*

The DAP reached 8370 m over multiple dives (reaching a maximum depth of 8377 m) to sample the bottom water from the Puerto Rico Trench during sea trials. The radiocarbon content of this bottom water was analyzed to determine its mean age (the time since its last exposure to the atmosphere). Previous studies extrapolated from data at distant sites to estimate the age of bathyal and/or abyssal water near the Puerto Rico Trench, with most estimates in the range of 250–300 yr (England 1995; Broecker 1979; Gebbie and Huybers 2012;

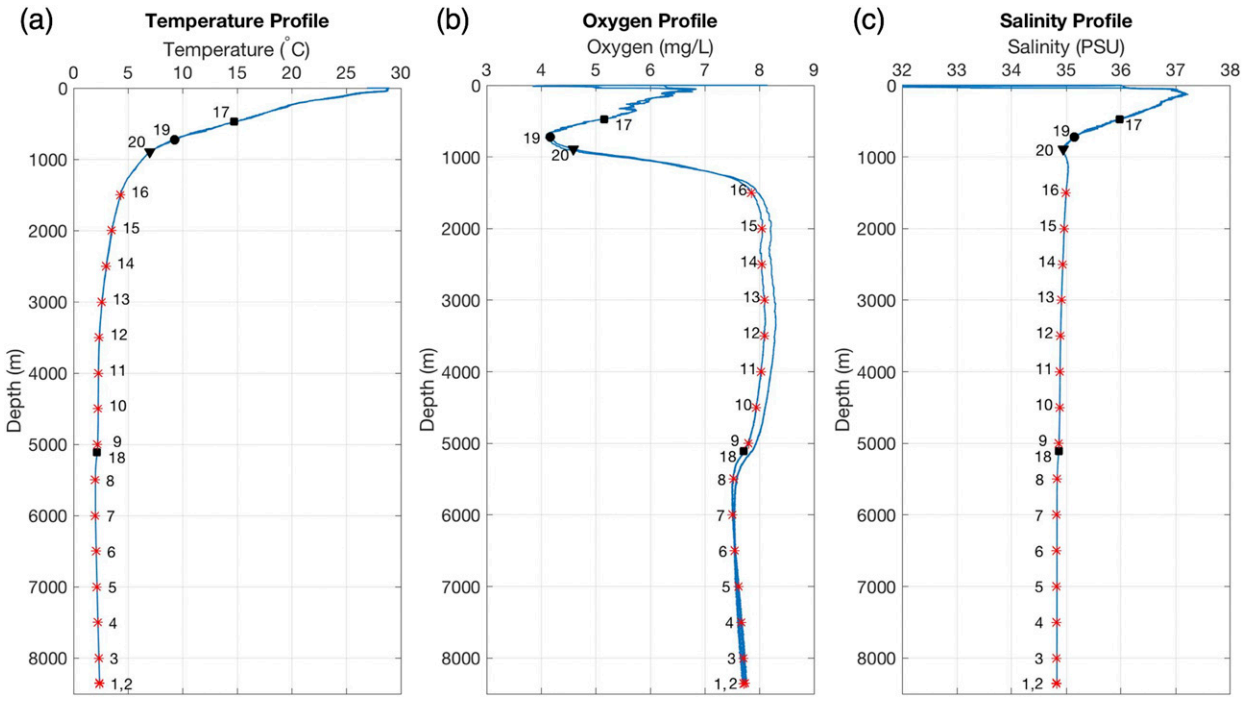

FIG. 7. Example of the combination of depth-distributed bottles (red asterisks) with supplemented adaptive bottles (black symbols). Bottles 17 and 18 are thermoclines, bottle 19 is the oxygen minimum, and bottle 20 is the salinity minimum.

Holzer et al. 2010; Matsumoto 2007). The estimates vary from study to study, because the local ratio of North Atlantic Deep Water (NADW) to Antarctic Bottom Water (AABW) is not precisely constrained, the estimation methods differ between studies, and the water depths for which age is estimated also differ between studies. The distinct properties of these deep-water sources are presented in Broecker et al. (1991, 1998) and Orsi et al. (1999).

The radiocarbon age of a sample is determined by measuring the radiocarbon ($\Delta^{14}C$) content of the water. Because the radiocarbon content of the surface ocean does not fully equilibrate with the atmosphere at sites of deep-water formation, the radiocarbon age of deep water is invariably older than the age of deep-water formation. To calculate the time since deep-water formation, this ''reservoir'' effect must be accounted for.

The reservoir value varies from one deep water mass to another. To determine the ventilation age of a deep sample, reservoir values need to be considered in proportion to the contribution of each water source (e.g., NADW and AABW). The proportion of the source waters can be determined from concentrations of conservative chemical tracers in the sample, such as SiO_2, NO, and PO_4^* (phosphate adjusted by Redfield ratio and O_2 consumption) (Broecker and Peng 1982).

Three different Niskin-bottle samples of bottom water from the Puerto Rico Trench were sent to the National Ocean Sciences Accelerator Mass Spectrometry facility at the Woods Hole Oceanographic Institution to be radiocarbon dated. The samples were fixed with $HgCl_2$ and refrigerated on board immediately following DAP recovery by the ship. The resulting radiocarbon ($\Delta^{14}C$) values are −113.15‰, −113.59‰, and −118.93‰ corresponding to radiocarbon ages of 900 ± 30, 905 ± 25, and 950 ± 25 yr, respectively.

To calculate the mean time since hadal water in the Puerto Rico Trench was last exposed to the atmosphere, these radiocarbon ages need to be corrected using a reservoir quantity that is adjusted for the AABW to NADW mixing ratio.

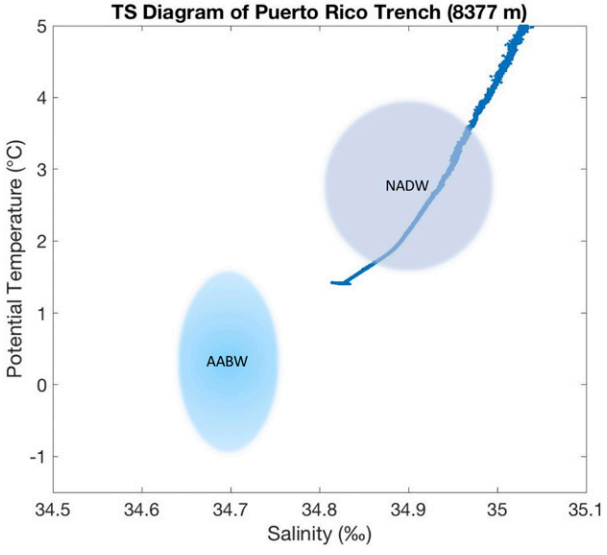

FIG. 8. A temperature–salinity plot of water below 1200-m depth. The small constant temperature plateau between the NADW and AABW is made up of water below 6000 m.

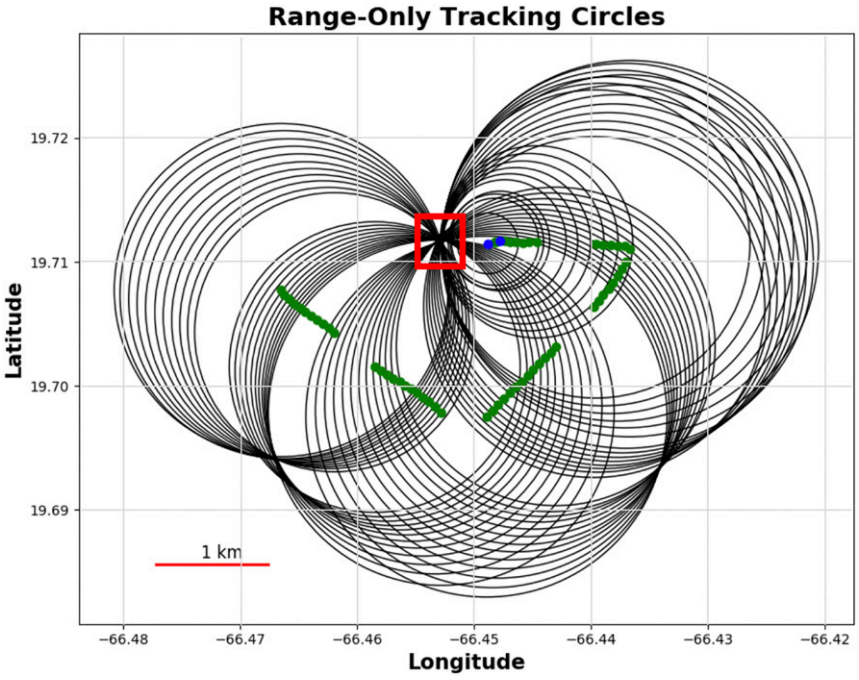

FIG. 9. Example of a successful range-only acoustic navigation system with properly set movement model and acoustic parameters to locate a deployed vehicle at 19°42.6′N by 66°27.47′W.

Figure 8 shows the temperature–salinity diagram of the bottom water, which is just outside the expected properties of NADW and indicates a small amount of AABW is likely present.

The tracer compounds of SiO_2 and NO used in Broecker (1979) to determine the deep water ratio between AABW and NADW were not measured in our samples. Instead, PO_4^* was calculated using the Redfield ratio of PO_4 and O_2 as described in Broecker and Peng (1982) and Broecker et al. (1998). This tracer indicates that hadal water in the Puerto Rico Trench is approximately 18% AABW and 82% NADW. Given reservoir values of −140‰ for AABW and −57‰ for NADW (Broecker et al. 1998; Gebbie and Huybers 2012), these percentages yield a reservoir value of −72‰ and a reservoir age of 600 yr for hadal water in the trench. When this reservoir age is subtracted from the samples' radiocarbon ages, the resulting estimate for the average of the three samples is 318 ± 25 yr. This age is slightly older than the estimates of 250 to 300 yr for overlying bathyal and abyssal water. This result suggests that hadal water in the Puerto Rico Trench turns over relatively rapidly, as predicted by analyses of hydrographic data in the Puerto Rico Trench region (van Haren and Gostiaux 2016; Schmidt and Siegel 2011) and western Pacific trench regions (Johnson 1998; Taira et al. 2004).

d. Range-only acoustic navigation

The range-only acoustic navigation system was used to locate the system while deployed. Figure 9 shows an example of successfully pinpointing the DAP where all the range circles overlap at 19°42.6′N by 66°27.47′W. The ship's path is also shown with the color indicating from which release the signal came. Typically, only one release provided a range at a given time. This is likely due to which side of the DAP has a direct path to the ship while the vehicle's foam pack is likely blocking the other. Other dropouts occurred without obvious explanation but were generally alleviated by moving the ship around the vicinity.

The main uncertainty with the tracking is caused by errors within the depth model or the bottom depth estimate. If the vertical speeds or start time are incorrect, the triangulation will estimate an incorrect horizontal distance. If the predicted descent speed is too fast, the model-estimated depth can become greater than the range and lead to an ill-conditioned solution. This error can occur when the ship is positioned over the DAP and the horizontal distance is short relative to vehicle's depth. If this occurs during operations, the operator is prompted to reset the model speeds or estimated depth until a consistent solution is found. In practice, adjustments to the model speeds were generally less than 10% of the anticipated value and mostly depended on how well the mass of a particular stack of ballast weights was known and if the configuration of the DAP had changed from prior deployments. In situations where the DAP configuration is consistent and prior dive data are available the model can be used with very little adjustment.

Another potential source of inaccuracy is ray bending due to sound speed changes with depth. To compensate for the significant sound speed change, the range is calculated using the actual sound speed profile, if known from a prior deployment, or an estimated sound speed profile at the deployment location. To determine the effect of ray bending throughout the profile ray traces were performed using the BELLHOP model

(Porter 2011) with the measured Puerto Rico Trench sound speed profile. This analysis confirmed that since the depth is much greater than the horizontal range the errors from ray bending are very small, remaining less than 0.3 m within 1.5 km of the actual position. As such, ray bending has little effect at the ranges of interest because the sound is hitting the speed gradients at high grazing angles. When the range is extended out to 10 km, the error grows to 20 m but still remains small enough to neglect for the real-time tracking.

4. Conclusions

The DAP was designed to bridge the sampling gap between shipboard CTDs and bottom landers, to enable effective sampling over the entire global range of seawater depths (0–11 km). The vehicle is able to autonomously operate to full ocean depth and target features of the water column at every depth while allowing other shipboard operations to be undertaken concurrently. This independent operation offers significant potential for saving time and expense during ship operations in bathyal, abyssal, and hadal waters. With a full set of Niskin bottles, the vehicle can retrieve significant quantities of water from great depths, which has traditionally been infeasible. This capability provides the means to collect and filter large quantities of water for a wide range of chemical and biological oceanographic measurements throughout the full range of seawater depths. The vehicle will provide an efficient means of sampling for measurements of deep-water ages. Collecting deep water at multiple stations will provide novel insight into the spatial variability of chemical and biological properties within a trench and between trenches. It will provide the means for identifying biological and chemical traits associated with the mixing of deep water masses, advancing insight into the origins of the microbial communities found in deep water, and testing the extent to which particles are actively colonized by pressure-adapted communities as they sink to progressively greater depths.

The vehicle travels at a nominal speed of $60\,\mathrm{m\,min^{-1}}$ through the water column, using drop weights for descent and syntactic foam for ascent. A CTD and an oxygen sensor are used to monitor the water column as the vehicle travels. Samples are taken with Niskin bottles while on the bottom or on the ascent. A sampling plan is loaded onto the vehicle to set the expected bottom/mission times, maximum depth, system aborts, and desired sample criteria.

The system was successfully deployed in the Puerto Rico Trench to a depth of 8370 m on multiple dives. The depth-specified and adaptive method were able to sample the gradients, maximums, and minimums of the water column on the ascent. The range-only tracking was effective but suffered some range dropouts, due to the operating depth and relative positioning of the ship and the vehicle. Water samples collected in the trench were radiocarbon dated, producing a mean age estimate of approximately 318 yr. Comparison of this result with estimates of water-mass ages at shallower depths suggests that hadal water in the trench is ventilated relatively rapidly. Oxygen profiles were also collected with a deep-rated SBE 43 sensor. This sensor matched the shipboard CTD cast data well for depths shallower than 5000 m. At greater depths, the sensor exhibited a distinct time-dependent hysteresis artifact that needed to be corrected in postprocessing. The correction largely addressed the hysteresis loop but left an unresolved trend of increasing oxygen concentration below 6000 m. This seems inconsistent with oxygen data collected in another deep trenches and suggests the correction is still not fully sufficient. To better resolve this issue, it will be necessary to collect addition profiles and pair those with measurements taken directly from the water collected in the Niskin samples at multiple depths. This would indicate the degree to which the correction deviates at deeper depths.

Improvements to the DAP for future deployments will include streamlining of mission planning and support for additional sensors. The vehicle has the capability for adding other adaptive sampling methods and sensors in a modular fashion. Because the current vehicle does not actually sit on the seafloor, some modifications to the drop weight system would be needed to position sensors closer to the sediment water interface. The operating endurance could be improved with better power management or sleep modes for the computer. The time series sampling on the bottom would benefit from a mechanism to flush the bottles prior to sampling, to ensure that the captured water has not been stagnant in the bottles before collection. In a quiescent deep environment, the ventilation of the open Niskin bottles may take considerable time without active flushing. We anticipate addressing many of these issues on planned expeditions back to the Puerto Rico Trench and Cayman Trough.

Acknowledgments. Funding for this project was provided by the National Science Foundation (NSF) Ocean Technology and Interdisciplinary Coordination (OTIC) under Award 1635466. The authors are grateful for the contribution of Todd Gregory, who completed the detailed mechanical design of the DAP. The authors are also thankful for the help provided by the crew of the R/V *Endeavor* during the two test cruises. The efforts of Robert Pockalny, Victoria Fulfer, David Smith, and Dennis Graham at sea and with the water samples are much appreciated. Alvaro Munoz Plominsky, Logan Peoples, Matthew Norenberg, and Douglas Bartlett provided and operated the deep-water pressure-retaining samplers and helped with the deep-water age analysis.

Data availability statement. Shipboard data collected during the test cruise (EN622) to the Puerto Rico Trench are archived at and available through Rolling Deck to Repository (https://doi.org/10.7284/134455). Data from the DAP deployments are archived at and available through BCO-DMO (https://www.bco-dmo.org/project/849231). The software for the DAP is built on open-source libraries, and the authors will share the code for use on other research projects upon request.

APPENDIX

Mission-Plan Setup

An example mission plan that lists the global parameters and three example Niskin bottles is shown below. The global parameters define the expected dive information, set conditional

flags, and define the latitude for the pressure-to-depth conversion. In this mission, bottle 1 will trigger at 8000-m depth. Bottle 2 will trigger at the minimum oxygen value deeper than 4000 m. Bottle 3 will trigger where the water temperature is 8°C. This text file can be generated by hand or with a graphical interface that lists all of the parameter options.

When the mission file is parsed at the start of a dive, any sample bottles with adaptive criteria are entered into a list. The system then buffers the sensor data feeds while the vehicle is descending. The recording stops when the system reaches the bottom. The criteria for each adaptive bottle are then used to determine a sample depth within the water column. These depths are then passed to the trigger actuation process and combined with any bottles already set for a specific depth in the mission plan.

The example mission plan looks like the following, with "#" indicating the beginning of a comment:

```
GLOBAL
  mis_timeout 00:10:00 # sec or min:sec or hr:min:sec
  bottom_time 00:02:00 # sec or min:sec or hr:min:sec
  max_depth 250 # positive meters
  enable_battery_abort 1 # (0) no (1) yes
  battery_cutoff 20 # percent capacity
  enable_ctd_abort 1 # (0) no (1) yes
  latitude 42 #latitude in decimal degrees
ENDGLOBAL

BOTTLE
  number 1
  trigger DEPTH
  value 8000
ENDBOTTLE

BOTTLE
  number 2
  trigger OXYGEN
  value MIN
  state UP
  range [4000:BOTTOM]
ENDBOTTLE

BOTTLE
  number 3
  trigger TEMPERATURE
  value 8
  state UP
ENDBOTTLE
```

REFERENCES

Bowen, A. D., and Coauthors, 2008: The Nereus hybrid underwater robotic vehicle for global ocean science operations to 11,000 m depth. *OCEANS 2008*, Quebec City, QC, Canada, IEEE, 1281–1290, https://doi.org/10.1109/OCEANS.2008.5151993.

——, and Coauthors, 2009: Field trials of the Nereus hybrid underwater robotic vehicle in the Challenger Deep of the Mariana Trench. *OCEANS 2009*, Biloxi, MS, IEEE, 2769–2778, https://doi.org/10.23919/OCEANS.2009.5422311.

Broecker, W. S., 1979: A revised estimate for the radiocarbon age of North Atlantic Deep Water. *J. Geophys. Res.*, **84**, 3218–3226, https://doi.org/10.1029/JC084iC06p03218.

——, and T.-H. Peng, 1982: Tracers in the sea. Columbia University Lamont-Doherty Geological Observatory Rep., 690 pp.

——, S. Blanton, W. M. Smethie Jr., and G. Ostlund, 1991: Radiocarbon decay and oxygen utilization in the deep Atlantic Ocean. *Global Biogeochem. Cycles*, **5**, 87–117, https://doi.org/10.1029/90GB02279.

——, and Coauthors, 1998: How much deep water is formed in the Southern Ocean? *J. Geophys. Res.*, **103**, 15 833–15 843, https://doi.org/10.1029/98JC00248.

Crease, J., T. Dauphinee, P. Grose, E. Lewis, N. Fofonoff, E. Plakhin, K. Striggow, and W. Zenk, 1988: The acquisition, calibration and analysis of CTD data. UNESCO Tech. Paper in Marine Science 54, 102 pp., https://www.jodc.go.jp/info/ioc_doc/UNESCO_tech/096989eb.pdf.

Cui, W., Y. Hu, W. Guo, B. Pan, and F. Wang, 2014: A preliminary design of a movable laboratory for hadal trenches. *Methods Oceanogr.*, **9**, 1–16, https://doi.org/10.1016/j.mio.2014.07.002.

Das, J., and Coauthors, 2015: Data-driven robotic sampling for marine ecosystem monitoring. *Int. J. Rob. Res.*, **34**, 1435–1452, https://doi.org/10.1177/0278364915587723.

Edwards, B., D. Murphy, C. Janzen, and N. Larson, 2010: Calibration, response, and hysteresis in deep-sea dissolved oxygen measurements. *J. Atmos. Oceanic Technol.*, **27**, 920–931, https://doi.org/10.1175/2009JTECHO693.1.

England, M. H., 1995: The age of water and ventilation timescales in a global ocean model. *J. Phys. Oceanogr.*, **25**, 2756–2777, https://doi.org/10.1175/1520-0485(1995)025<2756:TAOWAV>2.0.CO;2.

Fossum, T. O., and Coauthors, 2019: Toward adaptive robotic sampling of phytoplankton in the coastal ocean. *Sci. Robots*, **4**, eaav3041, https://doi.org/10.1126/scirobotics.aav3041.

Franks, P. J. S., and B. A. Keafer, 2003: Sampling techniques and strategies for coastal phytoplankton blooms. Manual on harmful marine microalgae, UNESCO Rep., Vol. 2, 51–76.

Gallo, N., J. Cameron, K. Hardy, P. Fryer, D. Bartlett, and L. Levin, 2015: Submersible- and lander-observed community patterns in the Mariana and New Britain Trenches: Influence of productivity and depth on epibenthic and scavenging communities. *Deep-Sea Res. I*, **99**, 119–133, https://doi.org/10.1016/j.dsr.2014.12.012.

Gamo, T., and K. Shitashima, 2018: Chemical characteristics of hadal waters in the Izu-Ogasawara Trench of the western Pacific Ocean. *Proc. Japan Acad.*, **94B**, 45–55, https://doi.org/10.2183/pjab.94.004.

Gebbie, G., and P. Huybers, 2012: The mean age of ocean waters inferred from radiocarbon observations: Sensitivity to surface sources and accounting for mixing histories. *J. Phys. Oceanogr.*, **42**, 291–305, https://doi.org/10.1175/JPO-D-11-043.1.

Hardy, K., J. Cameron, L. Herbst, T. Bulman, and S. Pausch, 2013: Hadal landers: The Deepsea Challenge ocean trench free vehicles. *Oceans 2013*, San Diego, CA, IEEE, 1060–1069, https://ieeexplore.ieee.org/document/6741368.

Holzer, M., F. W. Primeau, W. M. Smethie, and S. Khatiwala, 2010: Where and how long ago was water in the western North Atlantic ventilated? Maximum entropy inversions of bottle data from WOCE line A20. *J. Geophys. Res.*, **115**, C07005, https://doi.org/10.1029/2009JC005750.

Huang, A. S., E. Olson, and D. C. Moore, 2010: LCM: Lightweight communications and marshalling. *2010 IEEE/RSJ Int. Conf. on Intelligent Robots and Systems*, Taipei, Taiwan, IEEE, 4057–4062, https://doi.org/10.1109/IROS.2010.5649358.

Ishibashi, S., and Coauthors, 2008: A ROV "ABISMO" for the inspection and sampling in the deepest ocean and its operation

support system. *OCEANS 2008*, Kobe, Japan, IEEE, 405–410, https://doi.org/10.1109/OCEANSKOBE.2008.4530967.

Jamieson, A. J., T. Fujii, M. Solan, and I. G. Priede, 2009: HADEEP: Free-falling landers to the deepest places on Earth. *Mar. Technol. Soc. J.*, **43**, 151–160, https://doi.org/10.4031/MTSJ.43.5.17.

Johnson, G. C., 1998: Deep water properties, velocities, and dynamics over ocean trenches. *J. Mar. Res.*, **56**, 329–347, https://doi.org/10.1357/002224098321822339.

Kinsey, J. C., R. M. Eustice, and L. L. Whitcomb, 2006: A survey of underwater vehicle navigation: Recent advances and new challenges. *Seventh Conf. of Manoeuvring and Control of Marine Craft*, Lisbon, Portugal, IFAC, 12 pp., http://141.212.194.179/publications/jkinsey-2006a.pdf.

Kyo, M., E. Hiyazaki, S. Tsukioka, H. Ochi, Y. Amitani, T. Tsuchiya, T. Aoki, and S. Takagawa, 1995: The sea trial of "Kaiko," the full ocean depth research ROV. *OCEANS '95*, San Diego, CA, IEEE, 1991–1996, https://doi.org/10.1109/OCEANS.1995.528882.

Leonard, N. E., D. A. Paley, R. E. Davis, D. M. Fratantoni, F. Lekien, and F. Zhang, 2010: Coordinated control of an underwater glider fleet in an adaptive ocean sampling field experiment in Monterey Bay. *J. Field Robot.*, **27**, 718–740, https://doi.org/10.1002/rob.20366.

Lermusiaux, P. F. J., 2007: Adaptive modeling, adaptive data assimilation and adaptive sampling. *Physica D*, **230**, 172–196, https://doi.org/10.1016/j.physd.2007.02.014.

Linley, T. D., M. E. Gerringer, P. H. Yancey, J. C. Drazen, C. L. Weinstock, and A. J. Jamieson, 2016: Fishes of the hadal zone including new species, in situ observations and depth records of liparidae. *Deep-Sea Res. I*, **114**, 99–110, https://doi.org/10.1016/j.dsr.2016.05.003.

Mandić, F., N. Mišković, N. Palomeras, M. Carreras, and G. Vallicrosa, 2016: Mobile beacon control algorithm that ensures observability in single range navigation. *IFAC-PapersOnLine*, **49**, 48–53, https://doi.org/10.1016/j.ifacol.2016.10.320.

Matsumoto, K., 2007: Radiocarbon-based circulation age of the world oceans. *J. Geophys. Res.*, **112**, C09004, https://doi.org/10.1029/2007JC004095.

Millard, R. C., and K. Yang, 1993: CTD calibration and processing methods used at Woods Hole Oceanographic Institution. Woods Hole Oceanographic Institution Tech. Rep., 107 pp.

Momma, H., and Coauthors, 2004: Loss of the full ocean depth ROV Kaiko—Part 1: ROV Kaiko—A review. *14th Int. Offshore and Polar Engineering Conf.*, Toulon, France, International Society of Offshore and Polar Engineers, 191–193.

Nunoura, T., and Coauthors, 2015: Hadal biosphere: Insight into the microbial ecosystem in the deepest ocean on Earth. *Proc. Natl. Acad. Sci. USA*, **112**, E1230–E1236, https://doi.org/10.1073/pnas.1421816112

Orsi, A., G. Johnson, and J. Bullister, 1999: Circulation, mixing, and production of Antarctic Bottom Water. *Prog. Oceanogr.*, **43**, 55–109, https://doi.org/10.1016/S0079-6611(99)00004-X.

Peoples, L. M., and Coauthors, 2018: Vertically distinct microbial communities in the Mariana and Kermadec Trenches. *PLOS ONE*, **13**, e0195102, https://doi.org/10.1371/journal.pone.0195102.

——, M. Norenberg, D. Price, M. McGoldrick, M. Novotny, A. Bochdansky, and D. H. Bartlett, 2019: A full-ocean-depth rated modular lander and pressure-retaining sampler capable of collecting hadal-endemic microbes under in situ conditions. *Deep-Sea Res. I*, **143**, 50–57, https://doi.org/10.1016/j.dsr.2018.11.010.

Popa, D. O., A. C. Sanderson, R. J. Komerska, S. S. Mupparapu, D. R. Blidberg, and S. G. Chappel, 2004: Adaptive sampling algorithms for multiple autonomous underwater vehicles. *2004 IEEE/OES Autonomous Underwater Vehicles*, Sebasco, ME, IEEE, 108–118, https://doi.org/10.1109/AUV.2004.1431201.

Porter, M. B., 2011: The BELLHOP manual and user's guide: Preliminary draft. Heat, Light, and Sound Research, Inc., Tech. Doc., 57 pp., https://oalib-acoustics.org/AcousticsToolbox/Bellhop-2010-1.pdf.

Schmidt, W. E., and E. Siegel, 2011: Free descent and on bottom ADCM measurements in the Puerto Rico Trench, 19.77°N, 67.40°W. *Deep-Sea Res. I*, **58**, 970–977, https://doi.org/10.1016/j.dsr.2011.06.005.

Sea-Bird, 2014: SBE 43 dissolved oxygen (DO) sensor—Hysteresis corrections. Sea-Bird Application Note 64-3, 8 pp.

Showstack, R., 2014: Unmanned research vessel lost on deep sea dive. *Eos, Trans. Amer. Geophys. Union*, **95**, 168, https://doi.org/10.1002/2014EO200004.

Stutters, L., H. Liu, C. Tiltman, and D. J. Brown, 2008: Navigation technologies for autonomous underwater vehicles. *IEEE Trans. Syst. Man Cybern.*, **38C**, 581–589, https://doi.org/10.1109/TSMCC.2008.919147.

Taira, K., S. Kitagawa, T. Yamashiro, and D. Yanagimoto, 2004: Deep and bottom currents in the Challenger Deep, Mariana Trench, measured with super-deep current meters. *J. Oceanogr.*, **60**, 919–926, https://doi.org/10.1007/s10872-005-0001-y.

Tarn, J., L. M. Peoples, K. Hardy, J. Cameron, and D. H. Bartlett, 2016: Identification of free-living and particle-associated microbial communities present in hadal regions of the Mariana Trench. *Front. Microbiol.*, **7**, 665, https://doi.org/10.3389/fmicb.2016.00665.

UNOLS, 2015: UNOLS rope and cable safe working standards. Research vessel safety standards, 10th ed., University-National Oceanographic Laboratory Systems Doc., A-1–A-21.

Vaganay, J., P. Baccou, and B. Jouvencel, 2000: Homing by acoustic ranging to a single beacon. *OCEANS 2000*, Providence, RI, IEEE, 1457–1462, https://doi.org/10.1109/OCEANS.2000.881809.

van Haren, H., and L. Gostiaux, 2016: Convective mixing by internal waves in the Puerto Rico Trench. *J. Mar. Res.*, **74**, 161–173, https://doi.org/10.1357/002224016819594809.

Vinogradova, N., 1997: Zoogeography of the abyssal and hadal zones. *Adv. Mar. Biol.*, **32**, 325–387, https://doi.org/10.1016/S0065-2881(08)60019-X.

Yilmaz, N. K., C. Evangelinos, P. F. J. Lermusiaux, and N. M. Patrikalakis, 2008: Path planning of autonomous underwater vehicles for adaptive sampling using mixed integer linear programming. *IEEE J. Oceanic Eng.*, **33**, 522–537, https://doi.org/10.1109/JOE.2008.2002105.

Yoshida, H., 2009: Fundamentals of underwater vehicle hardware and their applications. *Underwater Vehicles*, A. V. Inzartsev, Ed., InTech, 557–582.